ACS OMEGA

Open Access

http://pubs.acs.org/journal/acsodf

Article

Nanoparticles of $Cs_{0.33}WO_3$ as Antibiofilm Agents and Photothermal Treatment to Inhibit Biofilm Formation

Min Yi Wong,[¶] Bor-Shyh Lin,[¶] Po-Sheng Hu, Tsung-Yu Huang, and Yao-Kuang Huang*

Cite This: *ACS Omega* 2024, 9, 28144−28154

Read Online

ACCESS | Metrics & More | Article Recommendations | Supporting Information

ABSTRACT: Metal oxide nanoparticles with photothermal properties have attracted considerable research attention for their use in biomedical applications. Cesium tungsten oxide ($Cs_{0.33}WO_3$) nanoparticles (NPs) exhibit strong absorption in the NIR region due to localized surface plasmon resonance, through which they convert light to heat; hence, they can be applied to photothermal treatment for bacteria and biofilm ablation. Herein, $Cs_{0.33}WO_3$ NPs were synthesized through solid-phase synthesis, and their physical properties were characterized through Zetasizer, energy dispersive X-ray spectroscopy, Fourier transform infrared spectrometer, and scanning and transmission electron microscopy (SEM and TEM, respectively). *Burkholderia cenocepacia* isolates were cultured in tryptic soy broth supplemented with glucose, and the biofilm inhibition and antibiofilm effects of the NPs were determined using a crystal violet assay and the Cell Counting Kit-8 (CCK-8) assay. The biofilm morphology and viability of NP-treated cultures after NIR irradiation were evaluated through SEM and confocal microscopy, respectively. The cytotoxicity of NPs to human macrophages was also assessed using the CCK-8 assay. The NPs effectively inhibited biofilm formation, with a formation rate of <10% and a viability rate of <50% at the concentration of ≥200 μg/mL. The confocal analysis revealed that NIR irradiation markedly enhanced biofilm cytotoxicity after treatment with the NPs. The assay of cytotoxicity to human macrophages demonstrated the biocompatibility of the NPs and NIR irradiation. In sum, the $Cs_{0.33}WO_3$ NPs displayed effective biofilm inhibition and antibiofilm activity at 200 μg/mL treatment concentration; they exhibited an enhancement effect under the NIR irradiation, suggesting $Cs_{0.33}WO_3$ NPs are a potential candidate agent for NIR-irradiated photothermal treatment in bacterial biofilm inhibition and antibiofilm.

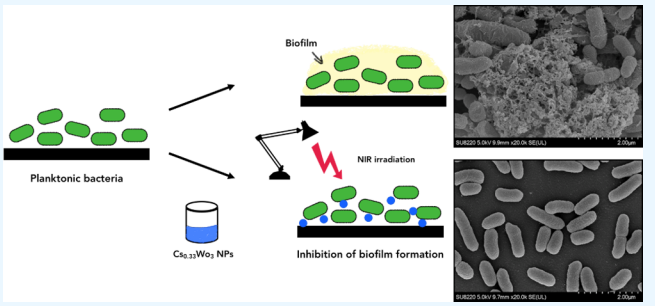

INTRODUCTION

Biofilms are structured microbial communities that adhere to almost all surfaces, and they contain sessile cells surrounded by a matrix of extracellular polymeric substances; this matrix is produced by the microorganisms themselves.[1] This bacteria−surface association is ubiquitous in most natural environments.[2] Microorganisms form biofilms to protect against various environmental stresses such as poor nutrients, changes in pH, and mechanical and shear forces. Biofilms enable microorganisms to tolerate harsh conditions and even develop resistance to antibiotics and host defense factors.[3] Bacterial biofilms can be beneficial or harmful to humans depending on the species and their localization. Biofilms are a medical threat and may cause numerous clinical problems. Biofilm-associated infections are a critical global problem and are increasing annually; moreover, their impact on healthcare services may be grossly underestimated. The biofilm formation on indwelling medical devices, including intravascular catheters, mechanical heart valves, urinary catheters, and orthopedic implants, can lead to serious, recalcitrant infections. Bacterial biofilms contribute to antibiotic resistance, which poses a challenge to the efficacy of traditional antibiotics. Biofilm eradication often requires antibiotic doses that are 100- to 1000-fold higher than those required for killing planktonic cells.[4] The inherent recalcitrance (i.e., tolerance and resistance) of sessile bacterial cells toward antimicrobial agents, such as antibiotics, is the key property leading to treatment failure and recurrence of chronic or local and systemic infections.[5]

Burkholderia cenocepacia is a member of the *B. cepacia* complex (BCC), which comprises a group of opportunistic pathogens that can cause nosocomial infections, including severe respiratory tract infections.[6] BCC members can survive and multiply in the presence of disinfectants, indwelling invasive medical devices, and antibiotic solutions, thus acting as a potential reservoir for infections in the hospital setting.[7] Because BCC organisms have innate resistance to a wide range of antimicrobial agents and they readily form biofilms, they are difficult to eradicate, and the infections caused by these

Received: February 6, 2024
Revised: June 4, 2024
Accepted: June 7, 2024
Published: June 18, 2024

bacteria are difficult to treat.[8] Therefore, alternative treatment options beyond traditional antibiotics are urgently needed to combat the resistance of bacterial biofilm infections.

The rapid advances in nanotechnology and the increasing use of nanoparticles (NPs) in biomedical applications offer viable solutions for identifying new antibiofilm agents. The use of NPs (nanoscale particles of size 1−100 nm) for the development of antimicrobial and antibiofilm agents have advantages over traditional antibiotics, such as their physicochemical properties of small size, large surface-to-volume ratio, and high stability. Metals have been used as antimicrobial agents since thousands of years.[9] The metal-based NPs use entirely different mechanisms of action from those described for traditional antibiotics, making it difficult for bacteria to develop resistance.[10] Metal-based nanomaterials with dimensions smaller than that of bacteria and their large surface-to-volume ratio allow strong interaction with the membrane of bacteria, causing its disruption, followed by damage of internal cellular structure, and ultimately leading to cell death, therefore facilitating strong antimicrobial effects on the bacteria and biofilm.[11] Metal and metal oxide NPs, such as silver (Ag), zinc oxide (ZnO), magnesium oxide (MgO), and titanium oxide (TiO_2), have demonstrated antimicrobial activity.[12−17]

Tungsten (W) (derived from Swedish: "tung + sten" = heavy stone) is a d-block transition metal in group 6 of the periodic table. Tungsten oxide (WO_3) is a versatile material that has been widely used as a semiconductor in applications such as photocatalysis, sensing, batteries, CO_2 reduction and pollutant degradation, electrochromic devices, cancer therapy, and even as antimicrobial agents.[18,19] Cesium tungsten oxide ($CsWO_3$) exhibits strong near-infrared (NIR) photoabsorption owing to its strong localized surface plasmon resonance (LSPR) effect; thus, $CsWO_3$ is an attractive candidate for photothermal applications.[20,21] In a previous study, $CsWO_3$ NPs were used in a photothermal antibacterial continuous flow microreactor, achieving over 99.9% antibacterial activity against *Staphylococcus aureus* and *Escherichia coli* over 30 days of continuous operation under NIR light irradiation.[22] Although a few studies have investigated the antibacterial ability of WO_3 and $CsWO_3$, no study has explored their antibiofilm effects. Therefore, in order to understand the therapeutic potential of $Cs_{0.33}WO_3$ NPs on antibiofilm in clinical application, the current study explored the biofilm inhibition and antibiofilm effects of $Cs_{0.33}WO_3$ NPs and their application for photothermal treatment on Gram-negative *B. cenocepacia*. In addition, the biocompatibility of $Cs_{0.33}WO_3$ NPs was explored by assaying their cytotoxicity to human macrophages.

MATERIALS AND METHODS

Synthesis of Cesium Tungsten Oxide ($Cs_{0.33}WO_3$) NPs. Tungsten bronze $Cs_{0.33}WO_3$ powder was synthesized via a solid-state reaction. In brief, ammonium tungstate [$(NH_4)_2WO_4$] (99% purity, Alfa Aesar, MA) and cesium chloride (CsCl) (99% purity, Alfa Aesar, MA) were taken at a mass proportion of 1:0.33, and these compounds were first separately dissolved in 100 mL of deionized (DI) water and then mixed in a beaker and stirred constantly at 250 rpm with a magnetic spinner for 1 h at 25 °C. The solution was then heated at 180 °C until the water completely evaporated, yielding a white dried powder, the precursor material. The white precursor powder was transferred to a quartz boat placed in a high-temperature furnace tube at a pressure of 0.08 Torr. The precursor was heated at 550 °C, and a gas mixture of H_2 and N_2 at a ratio of 90:10 Standard Cubic Centimeter per Minute (SCCM) was introduced to facilitate a redox reaction. After 1 h, the heating temperature was increased to 800 °C, and annealing was performed for 1 h with the N_2 gas flow adjusted to 100 SCCM. Finally, the furnace was turned off, and the dark blue micro (μ)-powder of $Cs_{0.33}WO_3$ was obtained after the quartz boat was cooled.[23]

Subsequently, the nanogrinding process was performed, in which 15 g of the $Cs_{0.33}WO_3$ μ-powder was mixed with 3.8 g of a copolymer-based dispersant agent (to prevent particle aggregation), 10 μL of an antifoaming agent, and adequate DI water to obtain a mixture solution of 150 g. The mixture solution was ground with 600 g of 0.1 mm zirconia (ZrO_2) beads for 4 h in the first grinding stage and with 0.05 mm ZrO_2 beads for another 4 h in the second grinding stage in the chamber of a nanogrinder equipment (Justnanotech Co., Taiwan) at a temperature of 15 °C and a rotational speed of 2,400 rpm. The final obtained solution was passed through a 0.22-μm pore filter for further characterization and experiments.

Characterization of $Cs_{0.33}WO_3$ NPs. The size distribution and zeta potential of $Cs_{0.33}WO_3$ NPs were evaluated using a Zetasizer Nano ZS90 (Malvern, Worcestershire, UK). The surface morphology and atomic composition of the NPs were determined through field-emission scanning electron microscopy (FE-SEM) (Hitachi SU8220, Japan) and energy dispersive X-ray spectroscopy (EDS) at an accelerating voltage of 10 kV, respectively. Moreover, the contour shape of $Cs_{0.33}WO_3$ NPs was assessed through high-resolution transmission electron microscopy (TEM) (Hitachi HT7800, Japan) at an accelerating voltage of 100 kV.[24] The infrared spectrum of $Cs_{0.33}WO_3$ NPs was obtained using a Fourier transform infrared (FTIR) spectrometer NIR-4850 (JASCO International Co., Ltd., Tokyo, Japan). The sample was mixed with potassium bromide (KBr) and pressed as pellets. Scans (256 scans) were recorded between 4000 and 400 cm^{-1} at a resolution of 16 cm^{-1}.

Bacterial Culture and Growth Conditions. The clinical isolates used in this study were *B. cenocepacia* CVS454 and CVS581, which were collected from Chiayi Chang Gung Memorial Hospital, a tertiary teaching hospital in Chiayi, Taiwan. This study was approved by its Institutional Review Board (IRB) (IRB No.: IRB 201801001B1). The isolates were routinely cultured on tryptic soy agar overnight at 37 °C and subcultured in tryptic soy broth (TSB) for 16 h at 37 °C.

Assessment of Biofilm Formation Ability and Biofilm Viability. The biofilm formation ability of the isolates was determined using the commercial Biofilm Formation Assay kit (Cat. no: B601−10, Dojindo, Japan). Briefly, biofilms were formed on the peg lid of the microtiter plate containing TSB supplemented with 0.25% w/v glucose (TSBg). Each well of the 96-well microtiter plate was inoculated with overnight culture at a dilution of 1:40, covered with a 96-peg lid, and incubated for 24 h at 37 °C under static conditions. The biofilm formed on the peg lid was quantified by measuring the absorbance of all samples at a wavelength of 590 nm by using a microplate reader.

To examine the biofilm inhibition ability and antibiofilm efficacy of the NPs, bacterial cultures were either untreated or treated with 10, 25, 50, 100, 250, 500, and 1000 μg/mL $Cs_{0.33}WO_3$ NPs for 24 h during inoculation. To assess the

https://doi.org/10.1021/acsomega.4c01212
ACS Omega 2024, 9, 28144−28154

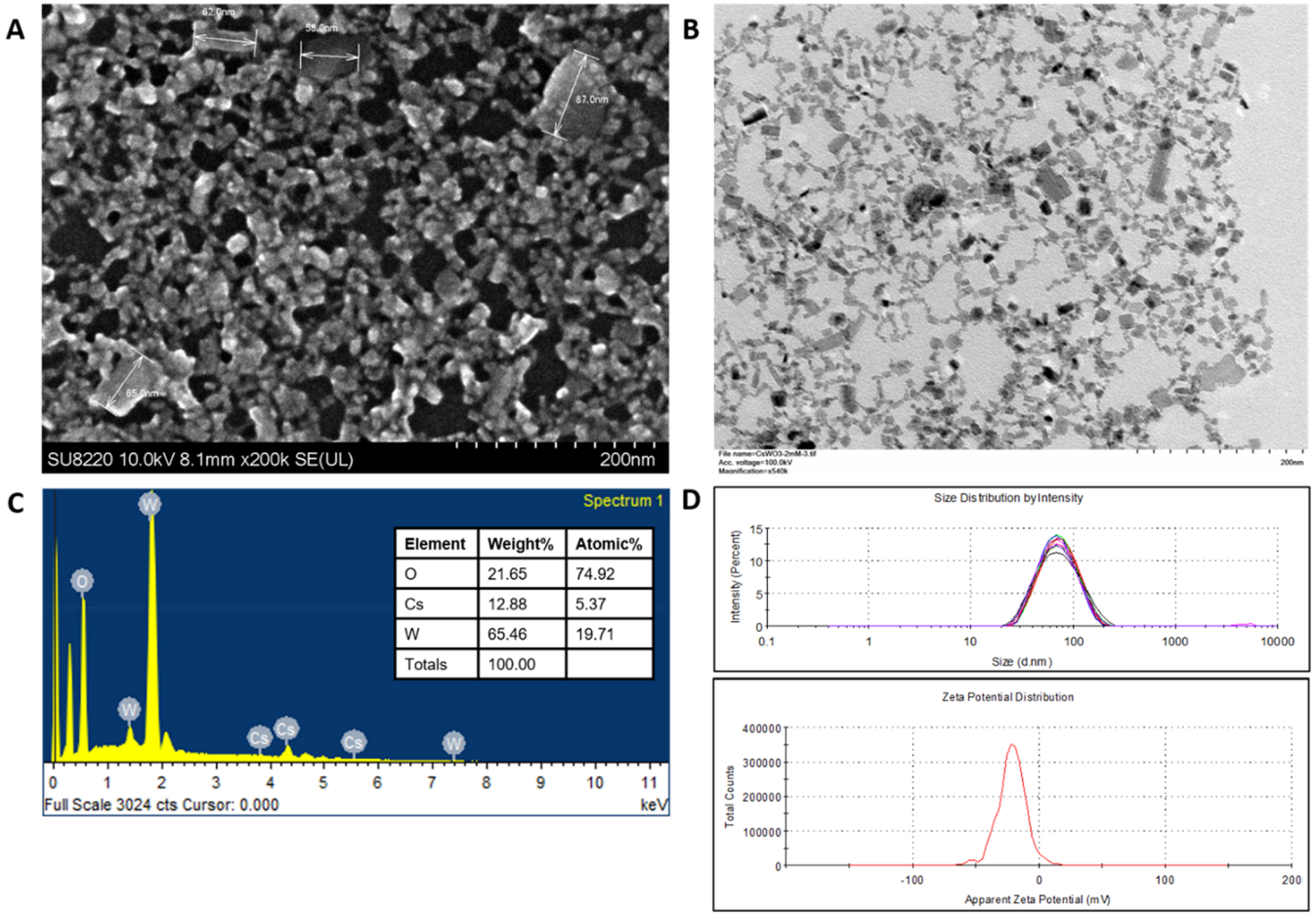

Figure 1. Characterization of $Cs_{0.33}WO_3$ nanoparticles. (A) SEM image. (B) TEM image. (C) EDS pattern depicting the atomic composition of $Cs_{0.33}WO_3$ NPs. (D) Size distribution and zeta potential of the NPs.

biofilm inhibition ability, after 24-h NP treatment, the biofilm formed on the peg lid was quantified using the Biofilm Formation Assay kit (Cat. no: B601−10, Dojindo, Japan) according to the manufacturer's protocol. To assess the antibiofilm efficacy of the NPs, the viability of the biofilm formed on the peg lid after 24-h NP treatment was determined using the commercial Biofilm Viability Assay kit (Cat. no: B603−10, Dojindo, Japan) following the manufacturer's protocol. The viable biofilm cells formed on the peg lid were also determined by the colony forming units (CFU) counting method. After 24-h NP treatment, the peg lid was washed with sterilized saline solution twice, transferred to a new 96-well microtiter plate containing saline, and subsequently placed in an ultrasonic bath for 15 min to detach the biofilm. Samples were then serially diluted 1:10 and 10 μL of each was spread on tryptic soy agar plates. Colonies were counted to evaluate antibiofilm activity after overnight incubation.

Photothermal Treatment and Antibiofilm Ability Analysis. The overnight culture was diluted to 1:1000 in TSB and grown for 6 h at 37 °C with shaking. A 30 mm glass bottom culture dish (Cat no.: PC209−0010, Simply) was inoculated with the 1:10 dilution of the subculture, and the subcultures were untreated or treated with either 100 or 200 μg/mL $CsWO_3$ NPs for 24 h. The biofilms formed on the culture dishes were irradiated with 150-W NIR light for 0 and 5 min. After photothermal treatment, the dishes were rinsed with sterilized physiological saline and assayed through staining by using the Filmtracer LIVE/DEAD Biofilm Viability Kit (Cat. no: L10316, Invitrogen, Molecular Probes, OR). A series of images were captured in the z section by using a Leica TCS SP5 II confocal microscope (Leica, Germany) with the objective Leica HCX PL APO 40.0 × 0.85 DRY lens (Leica, Germany). Three representative optical fields were examined for each sample. The viability of the biofilm was analyzed using the Biofilm Viability Checker, and 3D images of the biofilm were generated from the z-stack images by using the 3D viewer of ImageJ (Fiji).

Biofilm Morphology Visualization. To visualize changes in the morphology of the biofilm formed after treatment with $Cs_{0.33}WO_3$ NPs and NIR irradiation, the bacterial cultures were either untreated or treated with 100 and 200 μg/mL $Cs_{0.33}WO_3$ NPs and subsequently subjected to NIR irradiation. The biofilm formed on the surface of plastic coverslips was observed through SEM.[25] Overnight bacterial cultures diluted to 1:100 in TSBg were added on coverslips in the 35 mm Petri dish, followed by treatment with the NPs for 24 h. The samples were then exposed to 150-W NIR irradiation for 0 and 5 min. The samples were washed with phosphate-buffered saline three times and then fixed with 3% glutaraldehyde and 2% paraformaldehyde in 0.1 M cacodylate buffer (pH 7.4). The fixatives were removed by washing with 0.1 M cacodylate buffer, after which the samples were fixed in 1% osmium tetroxide in 0.1 M cacodylate buffer at 4 °C for 1 h. Then, the samples were dehydrated in a serial ethanol gradient (30%,

https://doi.org/10.1021/acsomega.4c01212
ACS Omega 2024, 9, 28144−28154

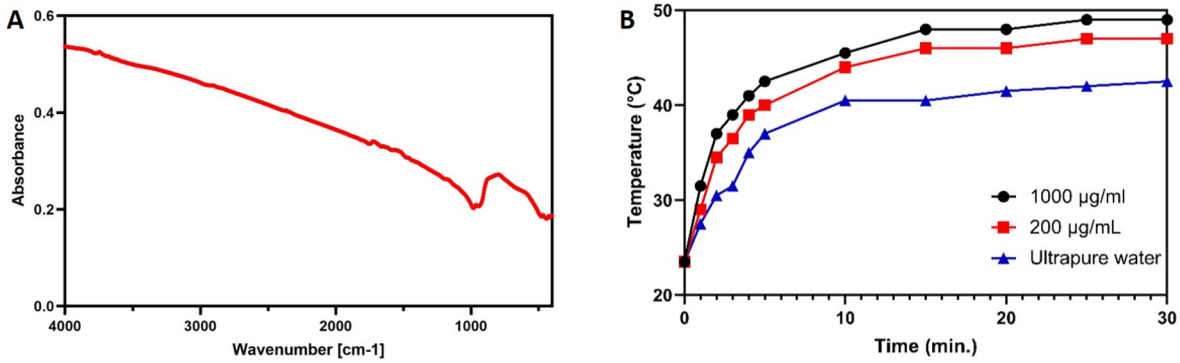

Figure 2. Optical and photothermal properties of $Cs_{0.33}WO_3$ nanoparticles. (A) FTIR analysis of $Cs_{0.33}WO_3$ NPs. (B) The time-course temperature measurement of different $Cs_{0.33}WO_3$ concentrations.

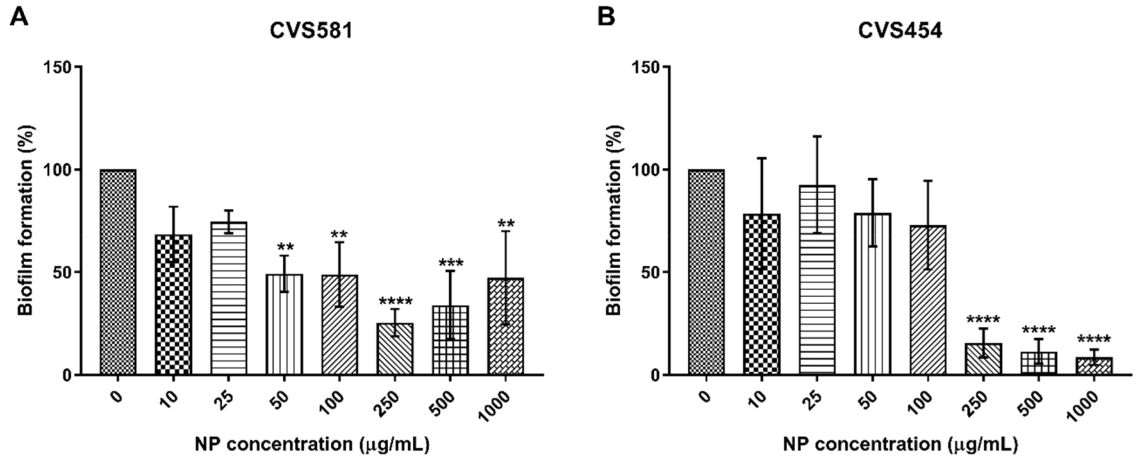

Figure 3. Biofilm formation ability of *B. cenocepacia* isolates after treatment with $Cs_{0.33}WO_3$ NPs for 24 h. The clinical isolates of *B. cenocepacia* (A) CVS581 and (B) CVS454 were treated with different concentrations (0−1000 μg/mL) of $Cs_{0.33}WO_3$ NPs, and the biofilms formed on the peg lids were assessed based on crystal violet staining. Data were normalized to the percentage of untreated biofilms in three independent experiments (n = 3) and are expressed as means ± standard deviations (SDs). Asterisks denote statistically significant decreases in biofilm formation rates compared with the untreated group (** $p < 0.01$, *** $p < 0.001$, **** $p < 0.0001$).

50%, 70%, 95%, and 100%), coated with platinum, and analyzed for biofilm morphology through FE-SEM (SU8220).

Cell Culture and Differentiation. The monocyte-like THP-1 cell line derived from the peripheral blood of a patient with acute monocytic leukemia was purchased from the Bioresource Collection and Research Center, Taiwan. The THP-1 cells were cultured in RPMI 1640 medium (ATCC modification) supplemented with 10% fetal bovine serum, 2-mercaptoethanol (0.05 mM), and 1% MycoZap Plus-CL (Cat. no: VZA-2012, Lonza, Switzerland) at 37 °C in a humidified atmosphere with 5% CO_2. The cells were further stimulated with 100 nM phorbol myristate acetate (PMA; Cat. no: P8139, Sigma-Aldrich, St. Louis, MO) for macrophage differentiation.

Cytotoxicity Assay. The Cell Counting Kit-8 (CCK-8) assay (Cat. no: C0005, TargetMol, Boston, MA) was used to assess the cell viability of the macrophages after exposure to $CsWO_3$ NPs. Briefly, the THP-1 cells were seeded in 96-well cell culture plates at a density of 0.4×10^5 cells/well, and their differentiation into macrophages was induced through the addition of PMA. Following 2-day differentiation, the cells were treated with a series of concentrations of $CsWO_3$ NPs (0, 100, 200, 400, and 800 μg/mL) for 1 day. At the end of NP treatment, the cells were incubated with fresh medium containing CCK-8 solution (1:10 in culture medium) for another 1−2 h at 37 °C. For photothermal treatment, macrophages treated with the NPs for 1 day were irradiated with 150-W NIR light for 5 min and then incubated with CCK-8 solution. Finally, the cytotoxicity of $CsWO_3$ was analyzed by measuring the absorbance of all samples at 450 nm by using a microplate reader. The viability of untreated cells was considered to be 100%.

Statistical Analysis. Statistical analyses were performed using one-way analysis of variance with GraphPad Prism 9.5 software. All results were calculated from the data of three independent experiments and are expressed as means ± standard deviations (SDs). In all experiments, cells treated with NPs were compared with untreated controls. A p value of <0.05 was considered statistically significant.

RESULTS

NP Characterization. As depicted in Figure 1A and B, the surface morphology and contour shape of $CsWO_3$ NPs were evaluated through SEM and TEM, respectively, and the results revealed that the particles were granular in nanoscale. Moreover, the results of the EDS analysis (Figure 1C) confirmed the atomic composition of $Cs_{0.33}WO_3$ with Cs, O, and W without other impurity peaks. The mean diameter and zeta potential of $Cs_{0.33}WO_3$ NPs, as measured using the Zetasizer equipment, were 63.12 ± 0.35 nm and −22.2 ± 1.35 mV, respectively (Figure 1D).

https://doi.org/10.1021/acsomega.4c01212
ACS Omega 2024, 9, 28144−28154

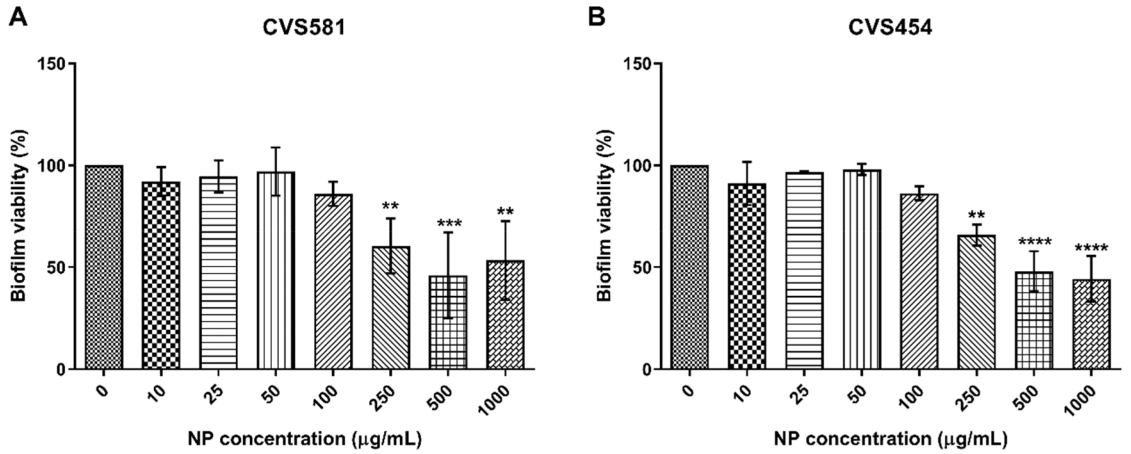

Figure 4. Biofilm viability of *B. cenocepacia* isolates after treatment with $Cs_{0.33}WO_3$ NPs for 24 h. The clinical isolates of *B. cenocepacia* (A) CVS581 and (B) CVS454 were treated with different concentrations (0−1000 μg/mL) of $Cs_{0.33}WO_3$ NPs, and the viability of the biofilms formed on the peg lids was determined using the CCK-8 assay. Data were normalized to the percentage of untreated biofilms in three independent experiments (n = 3) and are expressed as means ± standard deviations (SDs). Asterisks denote statistically significant decreases in biofilm viability rate compared with the untreated group (** $p < 0.01$, *** $p < 0.001$, **** $p < 0.0001$).

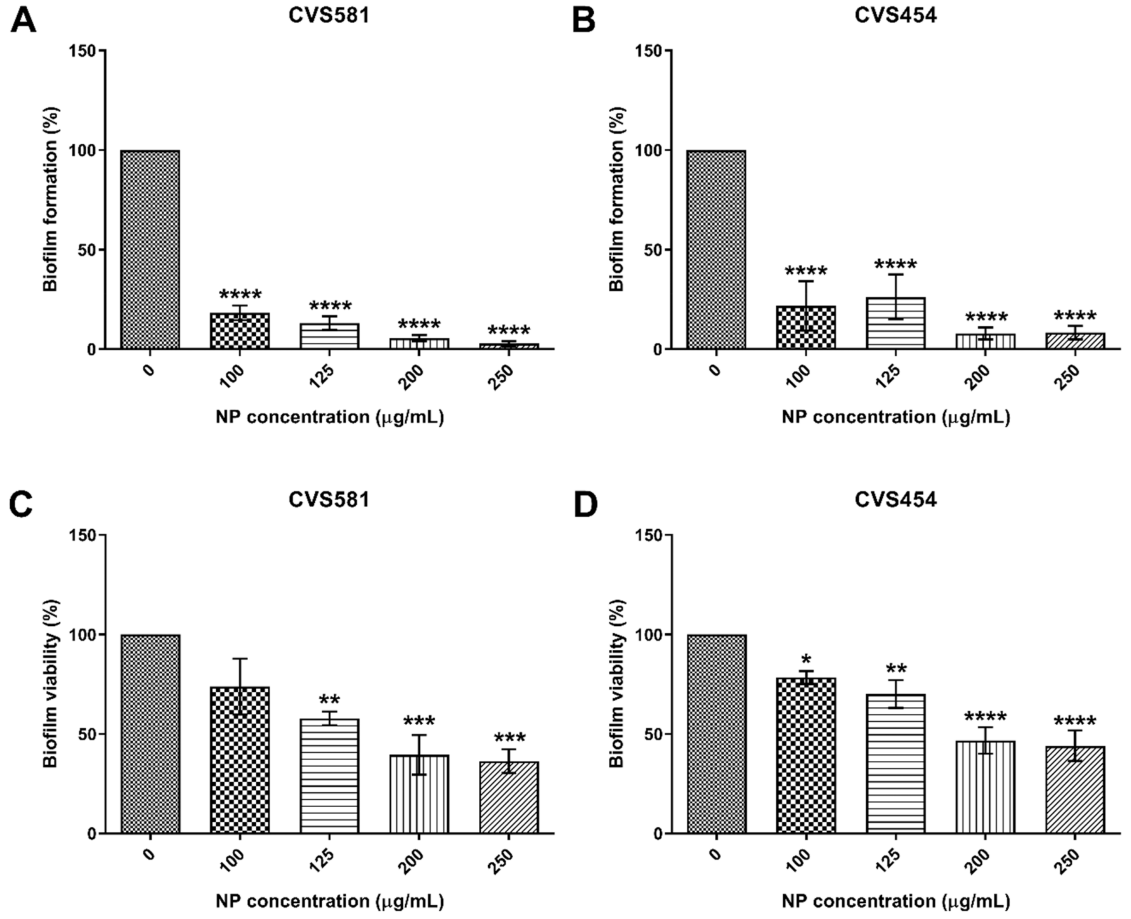

Figure 5. Biofilm formation and viability in *B. cenocepacia* isolates after treatment with $Cs_{0.33}WO_3$ NPs for 24 h. The clinical isolates of *B. cenocepacia* (A, C) CVS581 and (B, D) CVS454 were treated with different concentrations (0−250 μg/mL) of $Cs_{0.33}WO_3$ NPs, and the formation and viability of biofilms on the peg lids were determined using the crystal violet assay and CCK-8 assay, respectively. Data were normalized of the percentage of untreated biofilms in three independent experiments (n = 3) and are expressed as means ± standard deviations (SDs). Asterisks denote statistically significant decreases in the biofilm formation/viability rate compared with the untreated group (* $p < 0.05$, ** $p < 0.01$, *** $p < 0.001$, **** $p < 0.0001$).

An FTIR measurement was conducted over a wide wavelength range of 2500−25000 nm, equivalent to a wavenumber range of 4000−400 cm^{-1}, to analyze the spectral of $Cs_{0.33}WO_3$, as illustrated in Figure 2A. The absorption spectra of the $Cs_{0.33}WO_3$ NPs span the entire IR region.[26] A wide absorption band in the wavenumber range of 420−1000

https://doi.org/10.1021/acsomega.4c01212
ACS Omega 2024, 9, 28144−28154

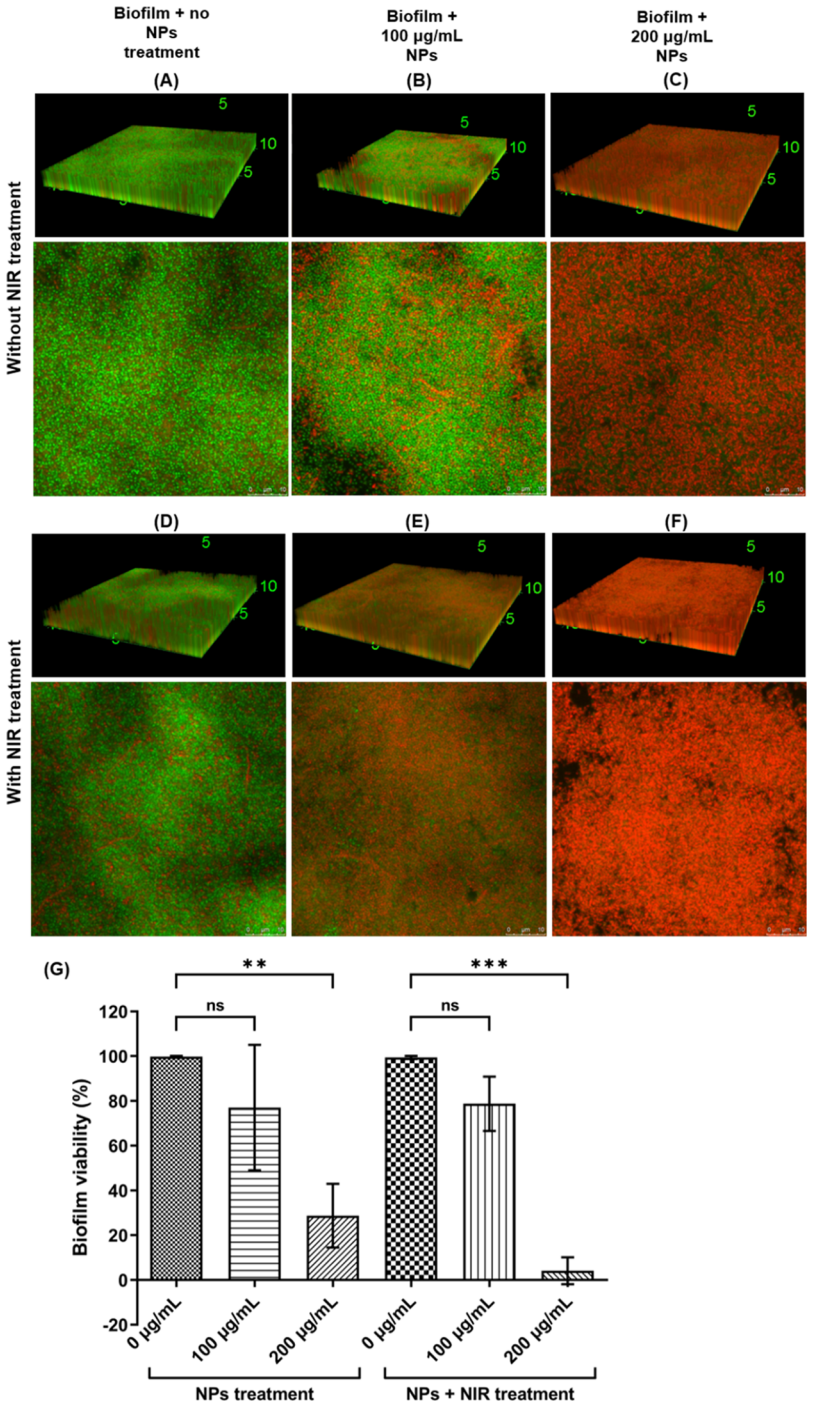

Figure 6. Confocal laser scanning microscopy images of *B. cenocepacia* biofilm after photothermal ablation in the absence or presence of $Cs_{0.33}WO_3$ NPs at different concentrations (6× zoom). The bacterial cultures were untreated (A, D) or treated with 100 μg/mL (B, E) and 200 μg/mL (C, F) $Cs_{0.33}WO_3$ NPs for 24 h followed by NIR irradiation (D, E, and F) for 5 min. The biofilm formed after 24-h treatment was stained with the Filmtracer LIVE/DEAD Biofilm Viability Kit; live cells exhibited green fluorescence, and dead cells exhibited red fluorescence. 3D images and the 2D view (upper and lower panel of each set, respectively) show the distribution of live and dead cells. Biofilm viability (percentage of live cells) (G) was quantified using the Biofilm Viability Checker and is expressed as mean ± standard deviation (SD) (n = 3).

cm^{-1} is observed, which can be attributed to the vibration modes of W−O bond, confirming the formation of tungsten oxide.[27] Figure 2B illustrates the profiles of temperature rise induced by NIR-irradiated NP solution as a function of NP concentration. The time-course temperature plot remains steady for at least 30 min, confirming the photothermal stability and durability of the materials.

Effect of NPs on Biofilm Formation Inhibition and Antibiofilm Abilities. The biofilm formation ability of two clinical isolates of *B. cenocepacia* was determined, and the effect of $Cs_{0.33}WO_3$ NPs on biofilm formation and antibiofilm abilities of these isolates was subsequently investigated. The isolates were found to be strong biofilm producers after the 24- and 48-h incubation periods. To determine the effect of the NPs on the biofilm formation inhibition ability of the bacterial

https://doi.org/10.1021/acsomega.4c01212
ACS Omega 2024, 9, 28144−28154

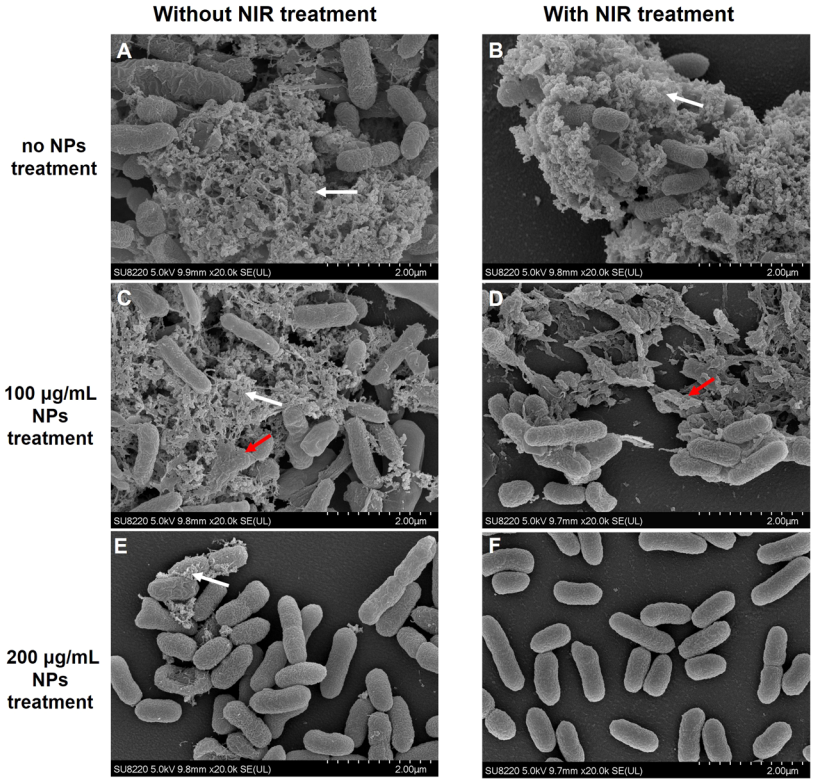

Figure 7. FE-SEM visualization of the *B. cenocepacia* biofilm after treatment with $Cs_{0.33}WO_3$ NPs and NIR irradiation. Bacteria were allowed to develop into a biofilm on coverslips for 1 day in the presence of different concentrations of $Cs_{0.33}WO_3$ NPs and then exposed to NIR irradiation. Micrograph depicting biofilms of bacteria that were untreated (A), treated with NIR irradiation alone (B), treated with different concentrations of $Cs_{0.33}WO_3$ NPs without NIR irradiation (C, E), and treated with $Cs_{0.33}WO_3$ NPs plus NIR irradiation (D, F). The white arrows indicate the extracellular matrix and red arrows indicate the structure or the morphological changes of cells.

cells, we treated the bacterial culture with different concentrations of the NPs during biofilm formation. Increasing the concentrations of the NPs significantly influenced the biofilm formation rate of the isolates (Figure 3). Specifically, treatment with 100 μg/mL NPs resulted in biofilm formation rates of 48.83% for CVS581 and 72.84% for CVS454. However, at NP concentrations of up to 250 μg/mL, the biofilm formation rate of the isolates markedly decreased to below 30% (25.38% and 15.54%, respectively). These findings suggested that $Cs_{0.33}WO_3$ NPs inhibited biofilm formation in a concentration-dependent manner, with effective inhibition observed at concentrations of up to 250 μg/mL.

Biofilm viability after NP treatment gradually decreased with increasing concentration; however, NPs at <100 μg/mL exhibited only slight antibiofilm effects against *B. cenocepacia* biofilm (Figure 4). For instance, at an NP concentration of 100 μg/mL, the biofilm viability of CVS581 and CVS454 was 85.99% and 86.20%, respectively, which decreased to 60.47% and 65.75% at 250 μg/mL. Furthermore, concentrations up to 500 μg/mL resulted in the destruction of more than 50% of the bacterial biofilm.

Given the substantial changes in the biofilm formation inhibition ability between the 100 and 250 μg/mL treatment concentrations, the lowest effective dose within 100 to 250 μg/mL range was determined. At 100 μg/mL, $Cs_{0.33}WO_3$ NPs inhibited biofilm formation, reducing the formation rate to <30%, while treatment concentrations of 200 μg/mL and higher led to rates of <10%, indicating nearly complete inhibition (Figure 5A and B). In addition, biofilm viability gradually reduced with increasing NP concentrations from 100 to 200 μg/mL, with more than 50% of the biofilm cells being destroyed, whereas the viabilities were closely similar for concentrations of 200 and 250 μg/mL (Figure 5C and D). Notably, a significant decrease in cell viability at 200 μg/mL treatment concentrations was also confirmed by CFU counting method (Figure S1). These results imply the high efficacy of $Cs_{0.33}WO_3$ NPs in inhibiting biofilm formation and their considerable cytotoxicity at a concentration of 200 μg/mL. Thus, in addition to predominantly inhibiting biofilm formation, $Cs_{0.33}WO_3$ NPs also play a role in killing biofilm cells.

Effect of Photothermal Treatment on the Antibiofilm Effects of $Cs_{0.33}WO_3$ NPs. The effect of photothermal treatment on the biofilm inhibition and antibiofilm effects of $Cs_{0.33}WO_3$ NPs was investigated through confocal microscopy and SEM. The confocal analysis demonstrated the antibiofilm effects of $Cs_{0.33}WO_3$ NPs (100 and 200 μg/mL) under NIR irradiation. The LIVE/DEAD Biofilm Viability kit provides a two-color fluorescence assay and was used to distinguish live and dead bacterial cells within the biofilm community based on membrane integrity. The SYTO9 green fluorescence dye penetrates healthy and damaged membranes, while propidium iodide red fluorescence dye only penetrates bacteria with damaged membranes. Bacteria with intact cell membranes (i.e., live) are stained fluorescent green, while those with damaged membranes (i.e., dead) are stained fluorescent red. As illustrated in Figure 6, untreated biofilm cells exhibited green fluorescence, while the biofilm cells treated with 100 μg/mL NPs exhibited a mixture of green and red fluorescence, indicating the presence of dead cells post-NP treatment. The

https://doi.org/10.1021/acsomega.4c01212
ACS Omega 2024, 9, 28144−28154

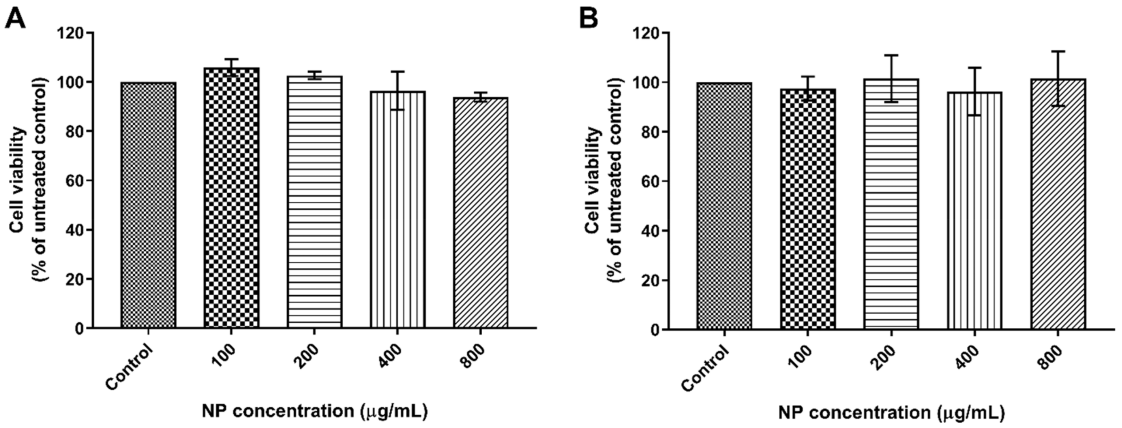

Figure 8. Cytotoxic effect of $Cs_{0.33}WO_3$ NPs and NIR irradiation on THP-1 macrophages. Cell viability of THP-1 macrophages after exposure to different concentrations of $Cs_{0.33}WO_3$ NPs (A) plus NIR irradiation (B) was analyzed using the CCK-8 assay. Data were normalized to the percentage of untreated cells and are expressed as means ± standard deviations (SDs).

biofilm cells treated with 200 μg/mL NPs predominantly exhibited red fluorescence, indicating the loss of membrane integrity and cell death. Consistent with the results of the biofilm viability assay, NP-treated samples, especially those treated with 200 μg/mL NPs, exhibited significantly lower biofilm viability than untreated samples, confirming the antibiofilm effects of $Cs_{0.33}WO_3$ NPs. Moreover, samples treated with NIR irradiation alone exhibited green fluorescence and similar cytotoxicity to untreated samples, indicating limited toxicity of NIR irradiation to *B. cenocepacia* biofilms. However, when the biofilm cells were treated with the NPs followed by NIR irradiation, they exhibited brighter red fluorescence compared to NP treatment alone. Moreover, with NIR irradiation, NPs at a concentration of 200 μg/mL could kill more than 90% of the biofilm cells; this result suggested that photothermal treatment enhanced the ability of the NPs to cause biofilm cell membrane damage and cell death.

Furthermore, the architecture and morphology of the biofilm upon treatment with $Cs_{0.33}WO_3$ NPs (100 and 200 μg/mL) and NIR irradiation were observed through SEM. In the untreated and NIR irradiation alone groups, bacterial cells were aggregated and covered with a mature biofilm structure (Figure 7, panels A and B). Bacterial cells treated with 100 μg/mL NPs were also aggregated but had a less dense extracellular matrix covering, and the additional photothermal treatment seemed to destroy the biofilm structure (panels C and D). Furthermore, bacteria treated with 200 μg/mL NPs predominantly appeared isolated, with only a few aggregated cells having an extracellular matrix covering. The additional NIR irradiation resulted in near-complete cell isolation and biofilm inhibition, indicating that NP and photothermal treatments inhibited bacterial aggregation and biofilm formation. Nonetheless, the growth pattern of bacterial cells treated with 100 μg/mL and 200 μg/mL NPs was similar to untreated bacterial cells, indicating no effect of NPs treatment on bacterial growth (Figure S2). Therefore, the imaging studies (confocal microscopy and SEM) provided insights into the potential inhibition of biofilm formation and antibiofilm effects of $Cs_{0.33}WO_3$ NPs and photothermal treatment.

Biocompatibility. Biocompatibility is crucial for NPs and photothermal agents, ensuring their safety for biological applications alongside their biofilm inhibition and antibiofilm effects. To evaluate the cytotoxicity of $Cs_{0.33}WO_3$ NPs (100–800 μg/mL), the viability of mammalian macrophages was assessed using the CCK-8 assay. Even at the highest concentration tested (800 μg/mL), the viability of cells remained above 80% after 1 day treatment with $Cs_{0.33}WO_3$ NPs, indicating the low cytotoxicity of $Cs_{0.33}WO_3$ NPs to macrophages (Figure 8). Moreover, the viability of NP-treated macrophages remained above 80% under NIR irradiation, confirming the safety of the NPs and photothermal treatment dosage for bacterial biofilm inhibition in biological application.

DISCUSSION

Because of the increasing problem of antibiotic resistance and the low efficacy of classical drugs and agents in eradicating bacterial biofilms, the use of inorganic nanomaterials as alternative agents has recently received considerable research attention. Various NPs of d-block transition metals and their oxides, such as Ag, CuO, ZnO, and TiO_2, have demonstrated diverse biological activities and are increasingly considered as antimicrobial and antibiofilm agents.[28,29] For example, CuO NPs were demonstrated to efficiently reduce biofilm formation by MRSA and *E. coli* in a dose-dependent manner.[30] At concentrations of >50 μg/mL, these NPs also inhibited biofilm formation by oral bacteria[31] and therefore can be considered potential biofilm inhibition agents. Tungsten oxide, an important transition metal oxide semiconductor, is widely used in biomedical applications such as in biosensor electrodes and as anticancer and antimicrobial agents due to its high photoactivity, sensitivity, selectivity, and biocompatibility.[32−35] Mathary et al.[36] revealed the antibacterial effects of tungsten oxide NPs at 2.0 wt % against *S. aureus*, resulting in nonviability for 83.7% of the *S. aureus* population. In this study, we assessed the biofilm inhibition effects of $Cs_{0.33}WO_3$ NPs and found that $Cs_{0.33}WO_3$ NPs can be used as effective biofilm inhibition agents at a concentration of ≥200 μg/mL (Figure 5).

Alkali-doped tungsten bronze is a nonstoichiometric metal oxide with the general structure M_xWO_3, where M is any alkali metal, such as K, Cs, Rb, and x is a variable <1.[37,38] For $x \leq 0.33$, the bronze M_xWO_3 (M = K, Cs, Rb) exhibits a hexagonal structure, in which the M ion is at the center surrounded by a six-membered ring channel formed by arrays of corner-linked WO_6 octahedra.[38,39] The NP assembly of M_xWO_3 exhibits a remarkable solar heat-shielding effect on absorption of broadband NIR light due to the LSPR of free electrons.[40,41] Because of the strong NIR absorptive properties, $Cs_{0.33}WO_3$

https://doi.org/10.1021/acsomega.4c01212
ACS Omega 2024, 9, 28144−28154

NPs can efficiently convert NIR light into heat and hence can be used with photothermal therapy. Robby et al.[42] demonstrated that $CsWO_3$-immobilized polymer dots exhibited high antibacterial activity against *E. coli* and *S. aureus* under NIR irradiation but negligible antibacterial activity in the absence of NIR irradiation. A recent study demonstrated that the combination of poly(vinyl alcohol) (PVA)/WO_3 films and NIR light irradiation [$(WO_3/PVA)_4$ + NIR] markedly improved the antibacterial activity of $(WO_3/PVA)_4$, yielding high antibacterial efficiency of approximately 90% and >90% against *E. coli* and *S. aureus*, respectively.[43] Similarly, in the current study, the confocal images (Figure 6) indicated that the bacterial biofilm treated with the NPs exhibited increasing red fluorescence (i.e., dead cells) in a concentration-dependent manner, but a markedly enhanced red fluorescence intensity was found in the presence of NIR irradiation, suggesting that NIR irradiation substantially improved the antibiofilm effects of $Cs_{0.33}WO_3$ NPs.

The antibacterial effects of NPs are highly dependent on their physiochemical properties, such as size, shape, surface morphology, and zeta potential. The zeta potential, also known as electrokinetic potential, is a measure of the net electrical charge on the surface of NPs and reflects their long-term stability.[44,45] It is a key feature of NPs that directly influences their biological activity, particularly their electrostatic interaction with bacteria or the bacterial biofilm. Most bacteria exhibit a negative zeta potential, which may be attributable to the dominance of negatively charged functional groups in macromolecules such as peptidoglycans, teichoic acids, teichuronic acids, lipopolysaccharides, phospholipids, proteins, and extracellular polysaccharides on the surface of the bacteria.[45,46] Studies have demonstrated that positively charged metal NPs interact with the negatively charged bacterial cell surface, which alters the zeta potential of the cells, thereby leading to membrane depolarization and bacterial cell damage; by contrast, negatively charged NPs exhibit markedly low antibacterial activity.[47] Nevertheless, the biofilm inhibition and antibiofilm effects of negatively charged $Cs_{0.33}WO_3$ NPs (zeta potential: − 22.2 ± 1.35 mV) herein may have caused the accumulation of NPs on the cell surface.[48] A differential change in the zeta potential affects the bacterial cellular physiology,[49] thus leading to cell death or interference in biofilm formation. In addition, the accumulation of NPs is beneficial for enhancing the dose of NIR irradiation in photothermal therapy combined with NP treatment.

Unlike bacteria, THP-1 macrophages were not sensitive to $Cs_{0.33}WO_3$ NPs, possibly because the negatively charged NPs are not as easily penetrating cells by electrostatic interaction between membrane glycoproteins and NPs as positively charged NPs.[50] Moreover, a previous study indicated that the negatively charged NPs do not affect the cell cycle.[51] The difference in the culture environment of bacteria and eukaryotic cells may also cause their difference in sensitivity to $Cs_{0.33}WO_3$ NPs. The biomolecules in a complete cell culture medium may compete with cell membrane lipids to adsorb onto the surface of NPs and therefore weaken the interaction of NPs with the cell membrane and enhance biocompatibility.[35]

CONCLUSIONS

The current study demonstrated the biofilm inhibition and antibiofilm effects of $Cs_{0.33}WO_3$ NPs on *B. cenocepacia* isolates when used alone or in combination with NIR irradiation. It also confirmed the biocompatibility of the NPs for human macrophages. $Cs_{0.33}WO_3$ NPs exerted biofilm formation inhibition and antibiofilm effects in a concentration-dependent manner, with nearly complete inhibition at the concentration of 200 μg/mL. The synergic effects of NIR irradiation and NP treatment resulted in enhanced biofilm inhibition and antibiofilm effects. These results suggest that $Cs_{0.33}WO_3$ NPs are a potential biologically safe photothermal-based biofilm inhibition agent.

ASSOCIATED CONTENT

Supporting Information

The Supporting Information is available free of charge at https://pubs.acs.org/doi/10.1021/acsomega.4c01212.

Detailed information on biofilm viability of *B. cenocepacia* isolates after NPs treatment and effect of $Cs_{0.33}WO_3$ NPs on *B. cenocepacia* isolates growth using colony forming unit counting method (PDF)

AUTHOR INFORMATION

Corresponding Author

Yao-Kuang Huang − *Division of Thoracic and Cardiovascular Surgery, Chiayi Chang Gung Memorial Hospital, Puzi City, Chiayi County 61363, Taiwan; College of Medicine, Chang Gung University, Taoyuan City 33302, Taiwan; Division of Thoracic and Cardiovascular Surgery, Chiayi Hospital, MOHW, Chiayi City 60096, Taiwan;* orcid.org/0000-0003-2699-2207; Phone: +886-975368209; Email: huang137@mac.com

Authors

Min Yi Wong − *Division of Thoracic and Cardiovascular Surgery, Chiayi Chang Gung Memorial Hospital, Puzi City, Chiayi County 61363, Taiwan; College of Photonics, National Yang Ming Chiao Tung University, Tainan City 71150, Taiwan*

Bor-Shyh Lin − *College of Photonics, National Yang Ming Chiao Tung University, Tainan City 71150, Taiwan*

Po-Sheng Hu − *College of Photonics, National Yang Ming Chiao Tung University, Tainan City 71150, Taiwan*

Tsung-Yu Huang − *Division of Infectious Diseases, Department of Internal Medicine, Chiayi Chang Gung Memorial Hospital, Puzi City, Chiayi County 61363, Taiwan; College of Medicine, Chang Gung University, Taoyuan City 33302, Taiwan*

Complete contact information is available at: https://pubs.acs.org/10.1021/acsomega.4c01212

Author Contributions

¶M.Y.W. and B.S.L. contributed equally to this manuscript. M.Y.W. and B.S.L. performed all experiments and conceived the manuscript. P.S.H. and T.Y.H. performed partial experiments, gave suggestions, reviewed, and edited writing. Y.K.H. designed experiments, directed the project, and reviewed writing. All authors have given approval to the final version of the manuscript and agreed on publication.

Funding

This work was supported by grant from the National Science and Technology Council of Taiwan under grant number 111−-2314-B-182A-015 - and Chang Gung Memorial Hospital, Chiayi, Taiwan under grant numbers CORPG6L0071-3 and CMRPG6P0251.

Notes

The authors declare no competing financial interest.

■ ACKNOWLEDGMENTS

This manuscript was edited by Wallace Academic Editing. We would like to acknowledge the Leica SP5 II confocal microscope service (support) provided by the Precious Instrumentation Core Laboratory, Chang Gung Memorial Hospital, Chiayi, and the SEM and TEM services provided by Microscope Core Laboratory, Chang Gung Memorial Hospital, Linkou. We also appreciate Professor Jen-Tsung Yang's laboratory for assisting with Zetasizer. We would like to thank Professor Ming-Fa Hsieh for the use of FTIR and useful help.

■ REFERENCES

(1) Donlan, R. M.; Costerton, J. W. Biofilms: survival mechanisms of clinically relevant microorganisms. *Clin Microbiol Rev.* **2002**, *15* (2), 167−193.
(2) Lindsay, D.; von Holy, A. Bacterial biofilms within the clinical setting: what healthcare professionals should know. *J. Hosp Infect* **2006**, *64* (4), 313−325.
(3) Costerton, J. W.; Lewandowski, Z.; Caldwell, D. E.; Korber, D. R.; Lappin-Scott, H. M. Microbial biofilms. *Annu. Rev. Microbiol.* **1995**, *49* (1), 711−745.
(4) Ceri, H.; Olson, M.; Stremick, C.; Read, R.; Morck, D.; Buret, A. The Calgary Biofilm Device: new technology for rapid determination of antibiotic susceptibilities of bacterial biofilms. *J. Clin Microbiol* **1999**, *37* (6), 1771−1776.
(5) Lebeaux, D.; Ghigo, J. M.; Beloin, C. Biofilm-related infections: bridging the gap between clinical management and fundamental aspects of recalcitrance toward antibiotics. *Microbiol Mol. Biol. Rev.* **2014**, *78* (3), 510−543.
(6) LiPuma, J. J. Update on the *Burkholderia cepacia* complex. *Curr. Opin Pulm Med.* **2005**, *11* (6), 528−533.
(7) Rastogi, N.; Khurana, S.; Veeraraghavan, B.; Yesurajan Inbanathan, F.; Rajamani Sekar, S. K.; Gupta, D.; Goyal, K.; Bindra, A.; Sokhal, N.; Panda, A.; et al. Epidemiological investigation and successful management of a *Burkholderia cepacia* outbreak in a neurotrauma intensive care unit. *Int. J. Infect Dis* **2019**, *79*, 4−11.
(8) Rhodes, K. A.; Schweizer, H. P. Antibiotic resistance in *Burkholderia* species. *Drug Resist Updat* **2016**, *28*, 82−90.
(9) Hobman, J. L.; Crossman, L. C. Bacterial antimicrobial metal ion resistance. *J. Med. Microbiol* **2015**, *64* (5), 471−497.
(10) Lee, N. Y.; Ko, W. C.; Hsueh, P. R. Nanoparticles in the Treatment of Infections Caused by Multidrug-Resistant Organisms. *Front Pharmacol* **2019**, *10*, 1153.
(11) Wang, L.; Hu, C.; Shao, L. The antimicrobial activity of nanoparticles: present situation and prospects for the future. *Int. J. Nanomedicine* **2017**, *12*, 1227−1249.
(12) Sondi, I.; Salopek-Sondi, B. Silver nanoparticles as antimicrobial agent: a case study on *E. coli* as a model for Gram-negative bacteria. *J. Colloid Interface Sci.* **2004**, *275* (1), 177−182.
(13) Azam, A.; Ahmed, A. S.; Oves, M.; Khan, M. S.; Habib, S. S.; Memic, A. Antimicrobial activity of metal oxide nanoparticles against Gram-positive and Gram-negative bacteria: a comparative study. *Int. J. Nanomedicine* **2012**, *7*, 6003−6009.
(14) Zhang, L.; Jiang, Y.; Ding, Y.; Povey, M.; York, D. Investigation into the antibacterial behaviour of suspensions of ZnO nanoparticles (ZnO nanofluids). *J. Nanopart. Res.* **2007**, *9* (3), 479−489.
(15) Leung, Y. H.; Ng, A. M.; Xu, X.; Shen, Z.; Gethings, L. A.; Wong, M. T.; Chan, C. M.; Guo, M. Y.; Ng, Y. H.; Djurisic, A. B.; et al. Mechanisms of antibacterial activity of MgO: non-ROS mediated toxicity of MgO nanoparticles towards *Escherichia coli*. *Small* **2014**, *10* (6), 1171−1183.
(16) Huang, Z.; Maness, P.-C.; Blake, D. M.; Wolfrum, E. J.; Smolinski, S. L.; Jacoby, W. A. Bactericidal mode of titanium dioxide photocatalysis. *J. Photochem. Photobiol. A Chem.* **2000**, *130* (2−3), 163−170.
(17) Simon-Deckers, A.; Loo, S.; Mayne-L'hermite, M.; Herlin-Boime, N.; Menguy, N.; Reynaud, C.; Gouget, B.; Carriere, M. Size-, composition-and shape-dependent toxicological impact of metal oxide nanoparticles and carbon nanotubes toward bacteria. *Environ. Sci. Technol.* **2009**, *43* (21), 8423−8429.
(18) Huang, Z. F.; Song, J.; Pan, L.; Zhang, X.; Wang, L.; Zou, J. J. Tungsten Oxides for Photocatalysis, Electrochemistry, and Phototherapy. *Adv. Mater.* **2015**, *27* (36), 5309−5327.
(19) Mardare, C. C.; Hassel, A. W. Review on the Versatility of Tungsten Oxide Coatings. *physica status solidi (a)* **2019**, *216* (12), 1900047.
(20) Manthiram, K.; Alivisatos, A. P. Tunable localized surface plasmon resonances in tungsten oxide nanocrystals. *J. Am. Chem. Soc.* **2012**, *134* (9), 3995−3998.
(21) Chen, C.-J.; Chen, D.-H. Preparation and near-infrared photothermal conversion property of cesium tungsten oxide nanoparticles. *Nanoscale Res. Lett.* **2013**, *8*, 1−8.
(22) Kim, Y. K.; Kang, E. B.; Kim, S. M.; Park, C. P.; In, I.; Park, S. Y. Performance of NIR-Mediated Antibacterial Continuous Flow Microreactors Prepared by Mussel-Inspired Immobilization of $Cs_{0.33}WO_3$ Photothermal Agents. *ACS Appl. Mater. Interfaces* **2017**, *9* (3), 3192−3200.
(23) Hu, P. S.; Chou, H. J.; Chen, C. A.; Wu, P. Y.; Hsiao, K. H.; Kuo, Y. M. Devising Hyperthermia Dose of NIR-Irradiated $Cs_{0.33}WO_3$ Nanoparticles for HepG2 Hepatic Cancer Cells. *Nanoscale Res. Lett.* **2021**, *16* (1), 108.
(24) Rashid, T. M.; Nayef, U. M.; Jabir, M. S.; Mutlak, F. A.-H. Synthesis and characterization of Au: ZnO (core: shell) nanoparticles via laser ablation. *Optik* **2021**, *244*, No. 167569.
(25) Kadhim, W. K. A.; Nayef, U. M.; Jabir, M. S. Polyethylene glycol-functionalized magnetic (Fe3O4) nanoparticles: a good method for a successful antibacterial therapeutic agent via damage DNA molecule. *Surf. Rev. Lett.* **2019**, *26* (10), No. 1950079.
(26) Liu, G.; Xu, J.; Li, R. Chemical and morphological mechanisms of synthesizing rectangular cesium tungsten bronze nanosheets with broadened visible-light absorption and strong photoresponse property. *Mater. Des* **2020**, *194*, 108955.
(27) Tehrani, F. S.; Ahmadian, H.; Aliannezhadi, M. Hydrothermal synthesis and characterization of WO_3 nanostructures: Effect of reaction time. *Mater. Res. Express* **2020**, *7* (1), 015911.
(28) Turner, R. J. Metal-based antimicrobial strategies. *Microb Biotechnol* **2017**, *10* (5), 1062−1065.
(29) Baptista, P. V.; McCusker, M. P.; Carvalho, A.; Ferreira, D. A.; Mohan, N. M.; Martins, M.; Fernandes, A. R. Nano-Strategies to Fight Multidrug Resistant Bacteria-"A Battle of the Titans. *Front Microbiol* **2018**, *9*, 1441.
(30) Agarwala, M.; Choudhury, B.; Yadav, R. N. Comparative study of antibiofilm activity of copper oxide and iron oxide nanoparticles against multidrug resistant biofilm forming uropathogens. *Indian J. Microbiol* **2014**, *54* (3), 365−368.
(31) Tabrez Khan, S.; Ahamed, M.; Al-Khedhairy, A.; Musarrat, J. Biocidal effect of copper and zinc oxide nanoparticles on human oral microbiome and biofilm formation. *Mater. Lett.* **2013**, *97*, 67−70.
(32) Yuan, S. J.; He, H.; Sheng, G. P.; Chen, J. J.; Tong, Z. H.; Cheng, Y. Y.; Li, W. W.; Lin, Z. Q.; Zhang, F.; Yu, H. Q. A photometric high-throughput method for identification of electrochemically active bacteria using a WO_3 nanocluster probe. *Sci. Rep* **2013**, *3*, 1315.
(33) Santos, L.; Silveira, C. M.; Elangovan, E.; Neto, J. P.; Nunes, D.; Pereira, L.; Martins, R.; Viegas, J.; Moura, J. J. G.; Todorovic, S.; et al. Synthesis of WO_3 nanoparticles for biosensing applications. *Sens Actuators B Chem.* **2016**, *223*, 186−194.
(34) Wen, L.; Chen, L.; Zheng, S.; Zeng, J.; Duan, G.; Wang, Y.; Wang, G.; Chai, Z.; Li, Z.; Gao, M. Ultrasmall Biocompatible WO_{3-x} Nanodots for Multi-Modality Imaging and Combined Therapy of Cancers. *Adv. Mater.* **2016**, *28* (25), 5072−5079.

https://doi.org/10.1021/acsomega.4c01212
ACS Omega 2024, 9, 28144−28154

(35) Duan, G.; Chen, L.; Jing, Z.; De Luna, P.; Wen, L.; Zhang, L.; Zhao, L.; Xu, J.; Li, Z.; Yang, Z.; et al. Robust Antibacterial Activity of Tungsten Oxide (WO_{3-x}) Nanodots. *Chem. Res. Toxicol.* **2019**, *32* (7), 1357−1366.
(36) Matharu, R. K.; Ciric, L.; Ren, G.; Edirisinghe, M. Comparative Study of the Antimicrobial Effects of Tungsten Nanoparticles and Tungsten Nanocomposite Fibres on Hospital Acquired Bacterial and Viral Pathogens. *Nanomaterials (Basel)* **2020**, *10* (6), 1017.
(37) Magnéli, A.; Blomberg, B. Contribution to the knowledge of the alkali tungsten bronzes. *Acta Chem. Scand* **1951**, *5*, 372−378.
(38) Dickens, P.; Whittingham, M. The tungsten bronzes and related compounds. *Quarterly Reviews, Chemical Society* **1968**, *22* (1), 30−44.
(39) Magnéli, A. Tungsten bronzes containing six-membered rings of WO_6 octahedra. *Nature* **1952**, *169*, 791−792.
(40) Takeda, H.; Adachi, K. Near infrared absorption of tungsten oxide nanoparticle dispersions. *J. Am. Ceram. Soc.* **2007**, *90* (12), 4059−4061.
(41) Adachi, K.; Asahi, T. Activation of plasmons and polarons in solar control cesium tungsten bronze and reduced tungsten oxide nanoparticles. *J. Mater. Res.* **2012**, *27* (6), 965−970.
(42) Robby, A. I.; Park, S. Y. Recyclable metal nanoparticle-immobilized polymer dot on montmorillonite for alkaline phosphatase-based colorimetric sensor with photothermal ablation of Bacteria. *Anal. Chim. Acta* **2019**, *1082*, 152−164.
(43) Wang, Q.; Wang, H.; Zhang, T.; Hu, Z.; Xia, L.; Li, L.; Chen, J.; Jiang, S. Antibacterial Activity of Polyvinyl Alcohol/ WO_3 Films Assisted by Near-Infrared Light and Its Application in Freshness Monitoring. *J. Agric. Food Chem.* **2021**, *69* (3), 1068−1078.
(44) Pan, H.; Marsh, J. N.; Christenson, E. T.; Soman, N. R.; Ivashyna, O.; Lanza, G. M.; Schlesinger, P. H.; Wickline, S. A. Postformulation peptide drug loading of nanostructures. *Methods Enzymol* **2012**, *508*, 17−39.
(45) Ferreyra Maillard, A. P. V.; Espeche, J. C.; Maturana, P.; Cutro, A. C.; Hollmann, A. Zeta potential beyond materials science: Applications to bacterial systems and to the development of novel antimicrobials. *Biochim Biophys Acta Biomembr* **2021**, *1863* (6), No. 183597.
(46) Bundeleva, I. A.; Shirokova, L. S.; Bénézeth, P.; Pokrovsky, O. S.; Kompantseva, E. I.; Balor, S. Zeta potential of anoxygenic phototrophic bacteria and Ca adsorption at the cell surface: Possible implications for cell protection from CaCO3 precipitation in alkaline solutions. *J. Colloid Interface Sci.* **2011**, *360* (1), 100−109.
(47) Arakha, M.; Saleem, M.; Mallick, B. C.; Jha, S. The effects of interfacial potential on antimicrobial propensity of ZnO nanoparticle. *Sci. Rep* **2015**, *5* (1), 9578.
(48) Kuyukina, M. S.; Makarova, M. V.; Pistsova, O. N.; Glebov, G. G.; Osipenko, M. A.; Ivshina, I. B. Exposure to metal nanoparticles changes zeta potentials of *Rhodococcus* cells. *Heliyon* **2022**, *8* (11), No. e11632.
(49) Ong, T. H.; Chitra, E.; Ramamurthy, S.; Ling, C. C. S.; Ambu, S. P.; Davamani, F. Cationic chitosan-propolis nanoparticles alter the zeta potential of *S. epidermidis*, inhibit biofilm formation by modulating gene expression and exhibit synergism with antibiotics. *PLoS One* **2019**, *14* (2), No. e0213079.
(50) Sukhanova, A.; Bozrova, S.; Sokolov, P.; Berestovoy, M.; Karaulov, A.; Nabiev, I. Dependence of Nanoparticle Toxicity on Their Physical and Chemical Properties. *Nanoscale Res. Lett.* **2018**, *13* (1), 44.
(51) Liu, Y.; Li, W.; Lao, F.; Liu, Y.; Wang, L.; Bai, R.; Zhao, Y.; Chen, C. Intracellular dynamics of cationic and anionic polystyrene nanoparticles without direct interaction with mitotic spindle and chromosomes. *Biomaterials* **2011**, *32* (32), 8291−8303.

https://doi.org/10.1021/acsomega.4c01212
ACS Omega 2024, 9, 28144−28154